Article

Fabrication of polydopamine/rGO Membranes for Effective Radionuclide Removal

Chuang Li, Zhan Li,* Zheng Wang, Kecheng Guan, Yu-Hsuan Chiao, Pengfei Zhang, Ping Xu, Ralph Rolly Gonzales, Mengyang Hu, Zhaohuan Mai, Tomohisa Yoshioka, and Hideto Matsuyama*

Read Online

ACCESS | Metrics & More | Article Recommendations | Supporting Information

ABSTRACT: In this work, a novel polydopamine/reduced graphene oxide (PDA/rGO) nanofiltration membrane was prepared to efficiently and stably remove radioactive strontium ions under an alkaline environment. Through the incorporation of PDA and thermal reduction treatment, not only has the interlayer spacing of graphene oxide (GO) nanosheets been appropriately regulated but also an improved antiswelling property has been achieved. The dosage of GO, reaction time with PDA, mass ratio of PDA to GO, and thermal treatment temperature have been optimized to achieve a high-performance PDA/rGO membrane. The resultant PDA/rGO composite membrane has exhibited excellent long-term stability at pH 11 and maintains a steady strontium rejection of over 90%. Moreover, the separation mechanism of the PDA/rGO membrane has been systematically investigated and determined to be a synergistic effect of charge repulsion and size exclusion. Results have indicated that PDA/rGO could be considered as a promising candidate for the separation of Sr^{2+} ions from nuclear industry wastewater.
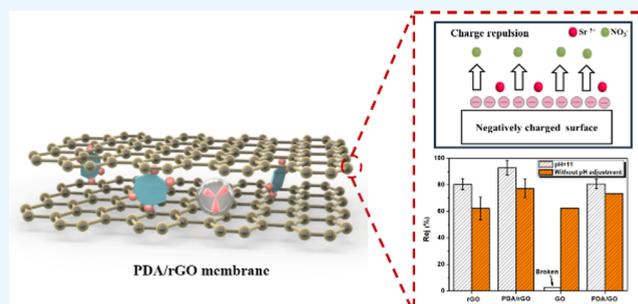
1. INTRODUCTION

The surging demand for energy has spurred the need for widespread harnessing of renewable energy resources, encompassing wind, thermal, solar, and nuclear energy. Notably, nuclear energy touts an exceptionally high energy density with a mere quantity of nuclear fuel yielding a substantial energy output. This distinctive feature enables nuclear power plants to maintain relatively compact physical footprints and occupy less land area. Moreover, nuclear energy exhibits reduced vulnerability to external influences like weather and climate, bolstering the power grid's reliability.

Despite the numerous advantages of nuclear energy, it remains imperative to address concerns such as the proper management of radioactive wastewater, as mishandling poses a significant threat to the neighboring soil and groundwater.[1] Comprising over 85% of the total volume of radioactive wastewater, the management of low-level radioactive wastewater (LLRW) is a prominent concern. Among the nuclides, strontium (^{90}Sr) stands out as a prevalent component featuring extended half-lives and substantial radiation emissions (^{90}Sr: $T_{1/2}$ = 28.79 A, E_β = 546 keV).[2,3] In addition, ^{90}Sr displays distinctive physical and chemical properties akin to calcium, facilitating its absorption by the human skeleton and heightening the risk of bone cancer or leukemia. As such, the quest for an efficient technique to remove ^{90}Sr from contaminated water becomes a pressing imperative in curtailing water pollution stemming from radionuclides.[4]

Several techniques have been developed for the removal of strontium ion (Sr^{2+}) from wastewater, including adsorption, chemical precipitation, coagulation/sedimentation, membrane filtration, and biological methods.[5,6] Among these, membrane-based separation emerges as a particularly advantageous choice for contaminant removal due to its reduced chemical consumption and ease of operation. In this realm, graphene-based membranes, including graphene and graphene oxide (GO) membranes, have gained considerable attention.[7] GO is composed of a carbon layer with oxygen-rich functional groups, e.g., functional hydroxyl, carboxyl, and epoxy groups.[8−11] When employed as membranes, GO membranes exhibit striking traits such as high hydrophilicity, as well as exceptional resistance to fouling and bacterial growth.[12−16] Yet, the structural integrity of the GO membrane encounters particular challenges in aqueous solutions, especially under alkaline conditions. Under acidic conditions, the oxygen-containing functional groups of the GO nanosheets are protonated. Therefore, the GO membrane exhibits good stability with appropriate interlayer spacings, resulting in
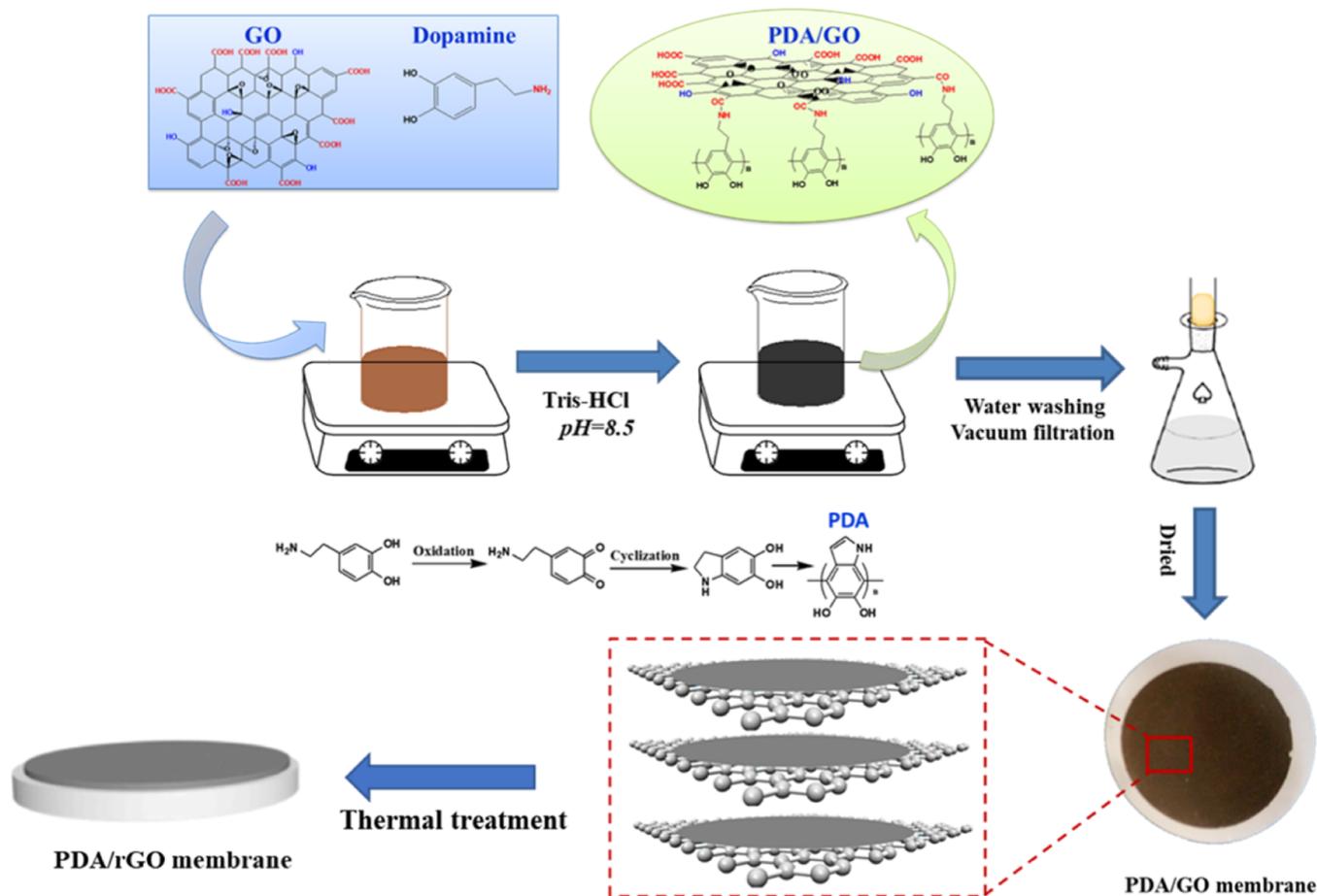
Figure 1. Schematic diagram of preparation of PDA/rGO composite membrane.

successful ion separation.[17,18] However, under alkaline conditions, the oxygen-containing functional groups in GO are deprotonated, causing the membrane to swell and severely hamper the separation performance.[19]

A prevailing strategy to improve the stability of a GO membrane is the incorporation of a GO compatible material. The structure of dopamine (DA) is rich in amine and hydroxyl groups, and DA can self-polymerize in aerobic and alkaline environments to form polydopamine (PDA). PDA can be easily coated onto various substrates and serves as an effective platform for surface modification.[20,21] PDA has been demonstrated to effectively enhance the stability of the GO membrane through covalent linking while also promoting a higher selectivity of the GO membrane. This selectivity is attributed to the presence of functional groups such as hydroxyl and amine groups, which serve as active sites for interacting with heavy metal ions and organic compounds.[22,23] Therefore, the combination of GO and PDA is expected to produce an antiswelling GO-based membrane with high selectivity. Nevertheless, the successful mitigation of swelling is achieved primarily when the PDA content significantly exceeds that of GO (by approximately 50 times). Yet, this benefit of reduced swelling comes at the cost of compromised membrane flux, owing to excessive PDA causing channel blockage. Conversely, at lower PDA loadings, the interlayer spacing of GO membranes expands, resulting in low salt rejection.[24,25] Thus, to mitigate the swelling of GO without compromising the membrane's performance, further modification in addition to PDA incorporation is necessary.

By reduction of the oxygen-containing functional groups in GO, the hydrophilicity of the GO membrane is diminished, and the swelling of GO nanosheets is relieved. At present, the prevailing reduction methods are chemical reduction, UV reduction, and thermal reduction.[26−28] Among these methods, thermal reduction is one of the most commonly employed posttreatment techniques for preparing reduced-GO (rGO) membranes. This approach significantly enhances the stability of GO-based membranes while allowing for fine-tuning of membrane selectivity.[29] However, the rGO membrane obtained by thermal treatment has poor rejection performance for strontium ions since thermal reduction treatment increases the hydrophobicity of the membrane. Strontium ions are likely to dehydrate when passing through a hydrophobic surface, causing a reduction in their diameter and facilitating their passage.[30] Therefore, thermal reduction treatment combined with PDA incorporation holds promise for further alleviating the swelling of GO membrane; the heightened hydrophobicity resulting from thermal reduction treatment, which may compromise strontium rejection performance, finds balance with the presence of hydrophilic PDA. To the best of our knowledge, there are no studies on enhancing strontium separation performance of PDA/GO membranes through thermal reduction posttreatment yet.

In this work, we have presented an integrated modification approach, by combining PDA incorporation and thermal reduction treatment, to tackle the challenging strontium separation in alkaline environments. This approach paves a potential avenue to enhance the overall efficacy of the

membrane system, addressing both the structural concerns associated with swelling and the performance challenges related to hydrophobicity. GO was first modified with DA and deposited onto the surface of poly(ether sulfone) (PES) support through vacuum filtration, resulting in a PDA/GO membrane. Subsequently, the PDA/GO membrane underwent thermal reduction to obtain the PDA/rGO membrane. The surface morphology, crystalline structure, and chemical composition of PDA/rGO composite membranes were characterized, and the successful preparation of the PDA/rGO membrane was confirmed. The separation performance of the PDA/rGO toward strontium ions (Sr^{2+}) has been investigated in a cross-flow separation unit. The influence of the dosage of GO, reaction time with PDA, mass ratio of PDA to GO, thermal treatment temperature, and solution pH on the Sr^{2+} separation performance was thoroughly examined, and the separation mechanism was discussed in detail. Additionally, we have conducted a rigorous assessment of the long-term strontium separation performance under alkaline conditions. Notably, the PDA/rGO membrane has exhibited remarkable stability in this challenging environment, a rarity among membranes modified using other reported methods. These findings not only highlight the potential utility of the PDA/rGO membrane for nuclear industry wastewater treatment but also propose an innovative approach to bolster the stability of GO-based membranes.

2. MATERIALS AND METHODS

2.1. Materials and Chemicals.
All chemicals were commercially available and used without further purification as follows. The GO suspension (4 mg mL^{-1} in H$_2$O), tris (hydroxymethyl) amino methane (Tris, 1 mol L^{-1}), DA hydrochloride (98.00 wt %), hydrochloric acid (HCl, 0.1 mol L^{-1}), and sodium hydroxide solution (NaOH, 0.1 mol L^{-1}) were purchased from Sigma-Aldrich Co., Ltd. PES microfiltration membranes (diameter of 47 mm, average pore size of 220 nm) were purchased from Merck Millipore Co., Ltd. strontium nitrate (Sr(NO$_3$)$_2$, 98.00 wt %), and strontium standard solution(1000 mg/L) were obtained from FUJIFILM Wako Pure Chemical Industries Co. Ltd. Ultrapure water was obtained from a Milli-Q system (Millipore, MA, USA).

2.2. Fabrication of the PDA/rGO Composite Membranes.
The synthesis process of the PDA/rGO membrane is illustrated in Figure 1. 22.5 mL of Tris−HCl buffer solution (10 mM, pH 8.5) was added into 2.5 mL of GO suspension and subjected to ultrasonic treatment. After 30 min, GO is exfoliated and a homogeneous suspension is obtained. Subsequently, a specific amount of DA hydrochloride was added to the suspension, and the mixture was stirred at room temperature for a duration ranging from 3 to 12 h, allowing complete modification of the GO with PDA. After the modification process, the PDA/GO composites were obtained by repeated centrifugation at 10,000 rpm and washing multiple times until the supernatant became transparent.

The PDA/GO composite was dispersed in 100 mL of water and deposited onto a (PES) substrate by vacuum filtration to prepare the PDA/GO membranes. The thickness of the PDA/GO membranes was regulated by the usage of PDA/GO composites during the deposition process. The prepared PDA/GO membranes were dried at 40 °C overnight prior to the thermal reduction treatment. The thermal treatment was performed in an oven at different temperatures. Specifically, the PDA/GO membranes were subjected to temperatures of

80 °C for 24 h and 120 °C for 30 min, respectively. For comparison, control samples of the pristine GO membrane and rGO membrane were prepared following the same procedure but without the addition of PDA; the control sample of the PDA/GO membrane was prepared without thermal treatment.

2.3. Characterization.
The morphology and chemical structures of the samples were examined on field-emission scanning electron microscopy (FESEM, JEM-2100F, JEOL Ltd., Japan), Fourier transform infrared spectroscopy (FTIR, Alpha Bruker, Billerica, MA, USA), and X-ray photoelectron spectroscopy (XPS, JSM-7100F, JEOL Ltd., Japan). The crystalline properties of the samples were identified by X-ray diffraction (XRD, RINT 2500 VHF, Rigaku Corp., Tokyo, Japan) using a Rigaku Ultima IV X-ray diffractometer with a Cu K$_\alpha$ source (40 kV, 20 mA). The surface zeta potentials of the membranes under different pH conditions were measured on a zeta potential analyzer (SurPASSTM3, Anton Paar, Graz, Austria). The surface roughness of the membranes was detected using atomic force microscopy (AFM; SPI3800 N; Hitachi Ltd., Tokyo, Japan).

2.4. Calculation of Interlayer Spacing.
The interlayer spacing of a GO-based membrane determines the size-selective separation performance. GO-based membranes reject the passage of molecules with a size larger than its interlayer spacing. The interlayer spacing of a GO-based membrane can be calculated from the XRD pattern by Bragg's law (eq 1).[31]

$$d = \frac{\lambda}{2\sin\theta} \tag{1}$$

where λ and θ represent the X-ray wavelength and diffraction angle, respectively.

2.5. Calculation of Surface Charge Density.
Surface charge density (Γ) is the quantity of charge per unit area, measured in moles per square meter (mol·m^{-2}), at any point on a surface charge distribution on a two-dimensional surface. The surface charge density can be calculated from the membrane zeta potential based on the following equation[32]

$$\Gamma = \frac{\sqrt{8C\varepsilon R}\sinh\left(\frac{|z|e\xi}{2kT}\right)}{eN_A} \tag{2}$$

where Γ (mol m^{-2}) is the membrane surface charge density, ξ (mV) is membrane zeta potential, C (mol m^{-3}) is the bulk electrolyte concentration(1 mol m^{-3}, KCl), z is the valence of the counterion, e is the elementary charge ($e = 1.60 \times 10^{-19}$ C), k is the Boltzmann's constant ($k = 1.38 \times 10^{-23}$ J/K), ε is the dielectric constant ($\varepsilon = 6.933 \times 10^{-10}$ F m^{-1}), and N_A is the Avogadro's constant ($N_A = 6.02 \times 10^{23}$ mol^{-1}).

2.6. Separation Performance Measurements for the Membranes.
The separation performance of the prepared membrane was evaluated using a self-designed cross-flow filtration apparatus (Figure 2). The Sr(NO$_3$)$_2$ aqueous solution (Sr^{2+} concentration = 10 mg/L) was used as the feed solution to simulate the LLRW. 200 mL of feed solution was constantly circulated in the membrane cell (effective filtration area = 7.07 cm^2) at a flow rate of 9.9 mL/min. Each membrane was compacted at 6 bar for 1 h with DI water to stabilize the permeate flux prior to the filtration test. The filtration test was carried out afterward at 3 bar.

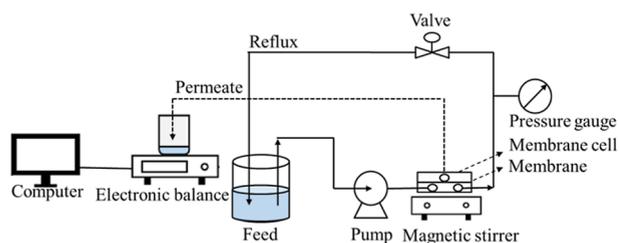The water permeance (L·m^{-2} h^{-1} bar^{-1}) is calculated according to the following eq 3

Figure 2. Schematic illustration of a membrane performance test device.

$$J = \frac{V}{A \times t \times P} \tag{3}$$

where V (L) is the volume of the permeate collected, A (m^2) is the surface area of the membrane, t (h) is the permeation time, and P is the transmembrane pressure.

The rejection ratios (Rej %) of Sr^{2+} are defined by the following eq 4

$$\text{Rej \%} = \frac{C_0 - C}{C_0} \times 100\% \tag{4}$$

where C_0 (mg·L^{-1}) and C (mg·L^{-1}) represent the concentration of strontium ion in the initial and collected solution, respectively. The ion concentrations of the initial feed solution and 2 h permeate samples were collected and measured by inductively coupled plasma emission spectroscopy (ICP-OES, Shimadzu, Japan). All the above experiments for separation performance tests were repeated three times, and the average values were used for analysis.

3. RESULTS AND DISCUSSION

3.1. Characterization of the Membranes. SEM was employed to observe the surface morphologies of the membranes. As shown in Figure 3, all the membranes exhibit a well-stacked structure, while GO and PDA/GO membranes display noticeable wrinkles. After thermal reduction treatment, the wrinkles on the membrane surfaces diminished (Figure 3d,e). Additionally, the thickness of the separation layer for the PDA/GO membrane is approximately 125 ± 5 nm, whereas thermal reduction yielded a thinner layer of the PDA/rGO membrane, measuring approximately 100 ± 5 nm (Figure 3c,f).

As shown in Figure 4, the incorporation of PDA and the subsequent thermal reduction treatment have exerted a noticeable influence on the surface roughness and hydrophilicity of the membranes. Upon the incorporation of PDA (in both PDA/GO and PDA/rGO membranes), the membrane surfaces have become smoother when compared to the GO and rGO membranes. However, owing to the inherent hydrophilic nature of PDA, the water contact angle still decreased after PDA incorporation despite the surface becoming smoother. As for thermal reduction treatment, the surface roughness of the reduced membranes (rGO and PDA/rGO membranes) is lower than that of the GO and PDA/GO membranes. Consequently, this reduction in surface roughness contributes to an increase in the water contact angle by thermal reduction treatment.

The chemical structures of the GO, PDA/GO, rGO, and PDA/rGO membranes were characterized by XPS (Figure 5). A distinct peak of N 1s (binding energy of 401.7 eV) has emerged in the XPS spectra of both the PDA/GO and PDA/rGO membranes, confirming the successful incorporation of PDA onto the GO nanosheets. Additionally, the O/C ratio has decreased after the thermal reduction treatment, indicating a partial reduction of oxygen-containing functional groups in the GO nanosheets. Peaking fitting result of C 1s peak has revealed the four components in GO: C=C/C−C at 284.8 eV; C−O at 286.8 eV; C=O at 287.5 eV; O−C=O at 288.6 eV.[33] An additional component, C−N at a binding energy of 285.7 eV, emerges in the peak fitting result for PDA/rGO. This C−N component can be attributed to the presence of PDA, providing further compelling evidence of the successful incorporation of PDA.[34]

3.2. Optimization of Preparation Conditions. *3.2.1. Influence of GO Dosage on Membrane Performance.* To determine the optimal GO dosage for membrane fabrication, membranes with varying amounts of GO were fabricated by vacuum filtration, and subsequently their performance in Sr^{2+} separation. As illustrated in Figure 6, Sr^{2+} rejection increases from 56.2% to 63.6%, as the GO dosage is raised from 0.028 to 0.042 mg/cm^2. Beyond this range, further increments in GO dosage fail to further enhance Sr^{2+} rejection, but instead lead to a substantial reduction in water permeance. This decline can be attributed to the increased membrane thickness associated with higher GO dosages.[35]
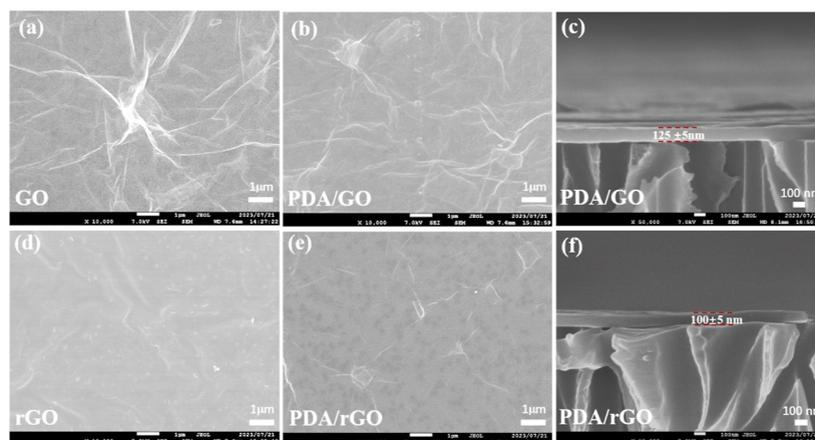

Figure 3. FESEM images of the surface of GO (a), PDA/GO (b), rGO (d), and PDA/rGO (e) membrane, the cross-section of PDA/GO (c) and PDA/rGO (f) membrane.
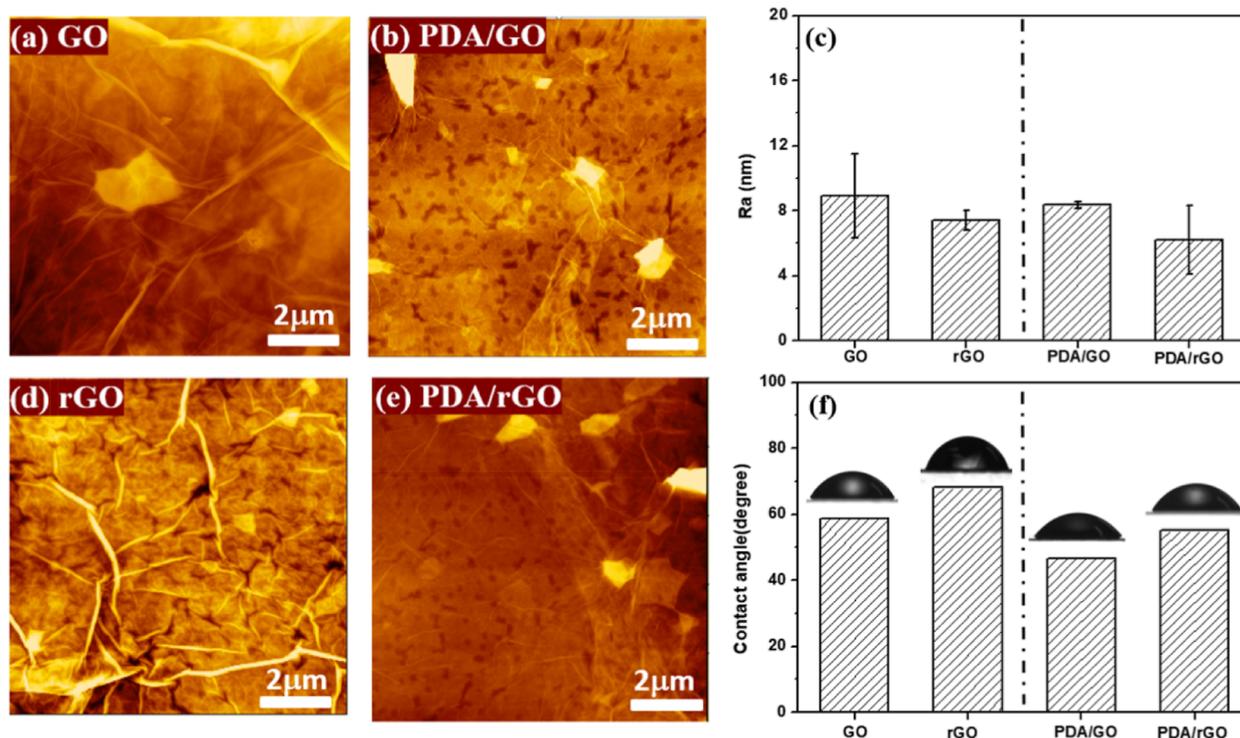
Figure 4. AFM images of the surface of GO (a), rGO (b), PDA/GO (d), and PDA/rGO (e) membrane, the surface average roughness (c), and contact angle (f) of the membrane.
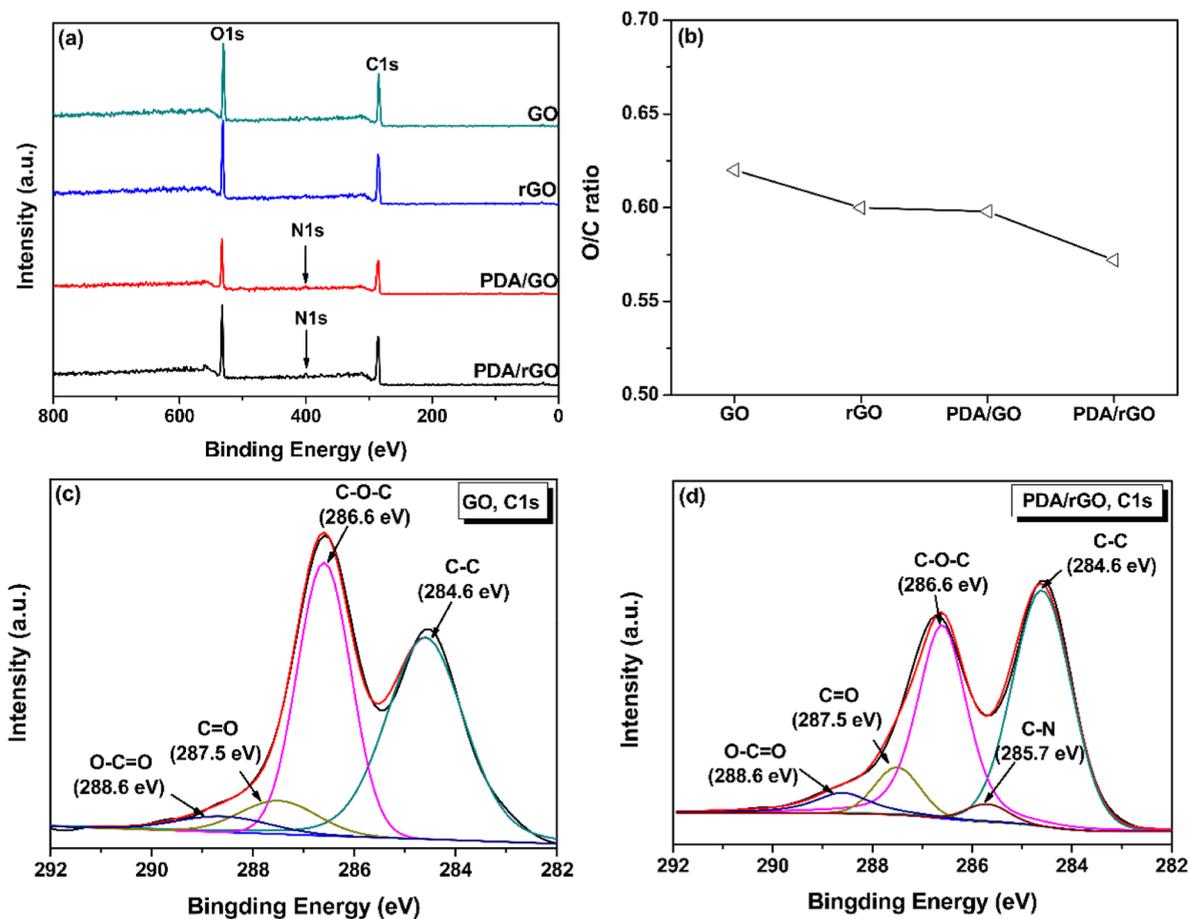

Figure 5. XPS spectra of GO, PDA/GO, rGO, and PDA/rGO: (a) wide scan spectra, (b) the O/C ratio, and C 1s spectra of (c) GO and (d) PDA/rGO, respectively.
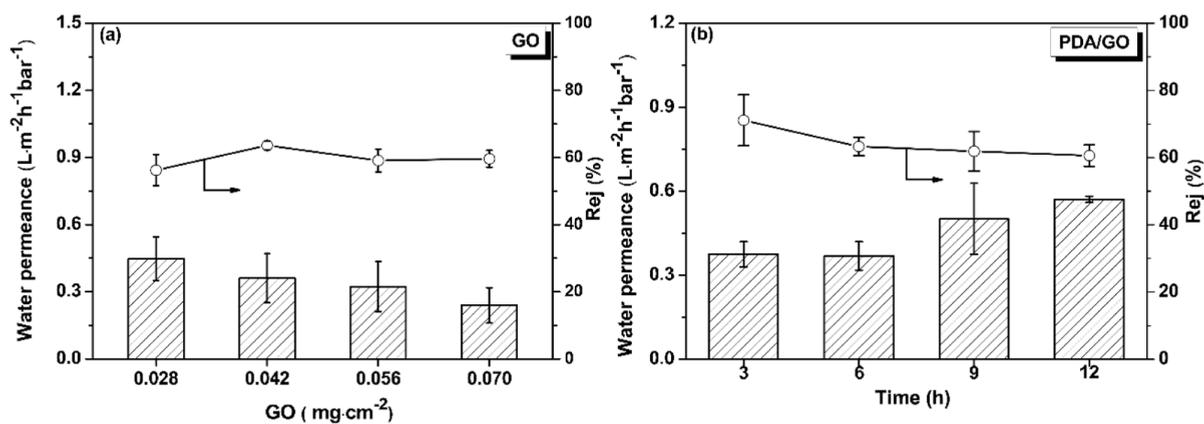
Figure 6. Performance of membranes prepared using varying GO dosage (a) and reaction time with PDA (b).
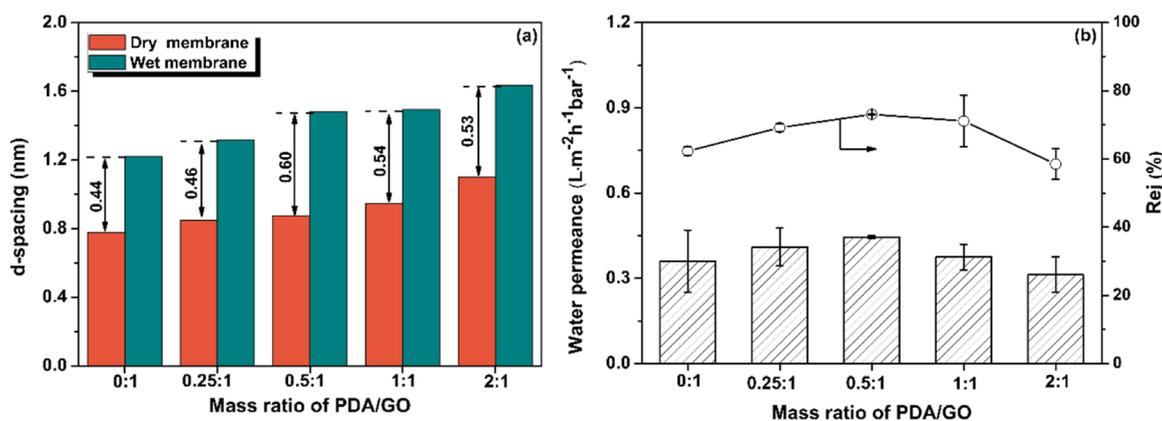

Figure 7. Interlayer spacing (a) and separation performance (b) of PDA/GO composite membranes with different PDA/GO ratios (the GO dosage and reaction time were fixed at 0.042 mg·cm^{-2} and 3 h, respectively).

Therefore, a GO dosage of 0.042 mg/cm^2 is determined to be optimal and is subsequently utilized. The membrane optimized at this dosage demonstrates a Sr^{2+} rejection rate of 63.6% and maintains a water permeance of 0.36 L·m^{-2}·h^{-1}·bar^{-1}.

3.2.2. Influence of Reaction Time of PDA and GO on Membrane Performance. Subsequently, the reaction time of PDA and GO has been optimized since the degree of PDA incorporation varies depending on the duration of the PDA and GO reaction. This variation is clearly discernible in the FTIR spectra (Figure S1), where the peak intensity of C=O (1774 cm^{-1}) obviously decreases with prolonged reaction time, reflecting the gradual consumption of C=O groups during the reaction with PDA. Furthermore, as the reaction time increases, both peaks of N−H (1576 cm^{-1}) and C−N (1485 cm^{-1}) have become more intense, providing concrete evidence of PDA incorporation.

Moreover, a noteworthy observation is the leftward shift in the characteristic diffraction peak of GO (Figure S2) as the reaction time extends (from 11.35° for pristine GO to 8.78° after a 12 h reaction). This shift indicates an expansion in the interlayer spacing between GO layers due to the incorporation of PDA, enlarging it from the original 0.78 nm in pristine GO to 1.01 nm after 12 h of reaction with PDA. The Sr^{2+} separation performance of membranes subjected to varying durations of the PDA and GO reaction has been evaluated (Figure 6b). With the extension of reaction time, there was an observed increase in water permeance of the membrane,

accompanied by a significant decrease in the Sr^{2+} rejection rate. This phenomenon can be attributed to the expansion of the interlayer spacing over prolonged reaction durations.[36] This expansion facilitates the passage of water molecules but compromises the membrane's ability to reject Sr^{2+} ions.

Hence, the optimal reaction time for PDA and GO is established as 3 h. This duration yields a water permeance of 0.375 L·m^{-2}·h^{-1}·bar^{-1} and a Sr^{2+} rejection of 71.1%.

3.2.3. Influence of PDA/GO Mass Ratio on Membrane Performance. To determine the optimal PDA usage, PDA/GO membranes with varying PDA/GO mass ratios, ranging from 0 to 2, have been prepared. As the PDA content increases, a concurrent enlargement in the interlayer spacing of the membrane, expanding from 0.850 nm for the 0.25:1 ratio to 1.102 nm for the 2:1 ratio, has been observed (Figure 7a and Figure S3). These findings align seamlessly with the aforementioned results, underscoring the direct correlation between increased PDA content and substantial enlargement of the interlayer spacing. Regarding Sr^{2+} separation performance (Figure 7b), both excessively high and excessively low PDA/GO mass ratios yield unsatisfactory results. A lower PDA/GO mass ratio results in a narrower interlayer spacing within the membrane, leading to reduced water permeance. Conversely, a higher PDA/GO mass ratio results in an excessively expanded interlayer spacing, which impairs the membrane's capacity to effectively reject Sr^{2+}. At the optimal PDA/GO mass ratio of 0.5:1, the membrane exhibited a water
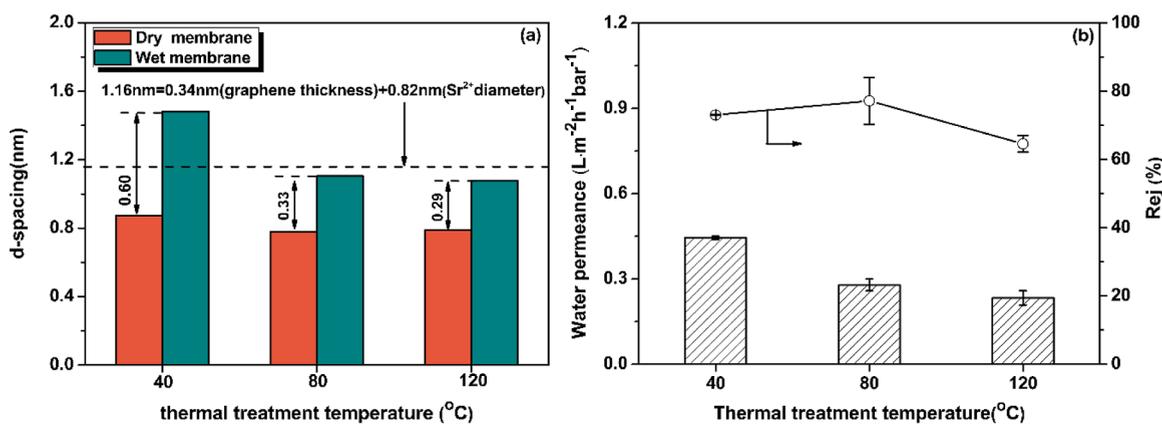
Figure 8. Interlayer spacing (a) and performance (b) of PDA/rGO composite membranes treated under different temperatures.
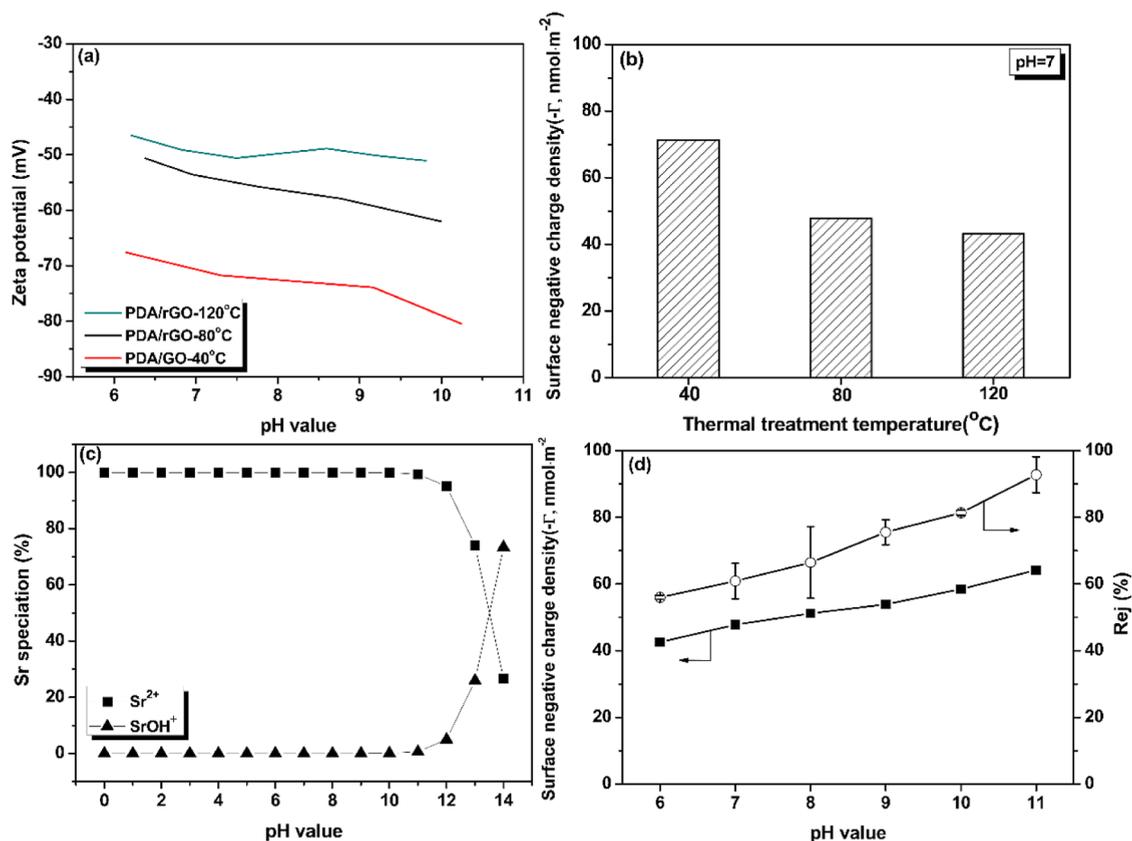

Figure 9. Zeta potential (a) and calculated surface negative charge density (b) of PDA/rGO membranes subjected to different thermal treatment temperatures. Composition analysis of the Sr^{2+} aqueous solution at different pH(c). Surface negative charge density and Sr^{2+} rejection under different pH values for PDA/rGO membrane (d).

permeance of 0.45 $L \cdot m^{-2} \cdot h^{-1} \cdot bar^{-1}$ and a Sr^{2+} rejection of 73.1%.

In summary, the optimization of GO dosage, reaction time, and PDA/GO mass ratio has resulted in a substantial enhancement in membrane performance (water permeance of 0.45 $L \cdot m^{-2} \cdot h^{-1} \cdot bar^{-1}$ and Sr^{2+} rejection of 73.1%) compared to that of pristine GO (water permeance of 0.36 $L \cdot m^{-2} \cdot h^{-1} \cdot bar^{-1}$ and Sr^{2+} rejection of 63.6%). However, the application of this membrane for Sr^{2+} separation remains challenging due to insufficient rejection. To investigate the underlying cause of this unsatisfactory separation performance, XRD measurements were performed on the wetted membranes to calculate the interlayer spacing of the membranes when in contact with

water.[37] Theoretically, a GO-based membrane can achieve Sr^{2+} separation via a size-exclusion mechanism when the interlayer spacing is less than 1.16 nm. This value is equivalent to the sum of the hydrated diameter of Sr^{2+} (0.82 nm) and the thickness of a graphene layer (0.34 nm).[38] As shown in Figure 7a, the interlayer spacing of the membrane, although small in its dry state, undergoes significant expansion when it swells. This excessively enlarged interlayer spacing hampers Sr^{2+} rejection significantly. Therefore, it is necessary to develop effective methods for mitigating the swelling of the GO-based membranes.

3.2.4. Influence of Thermal Treatment Temperature on Membrane Performance. The swelling of GO-based mem-
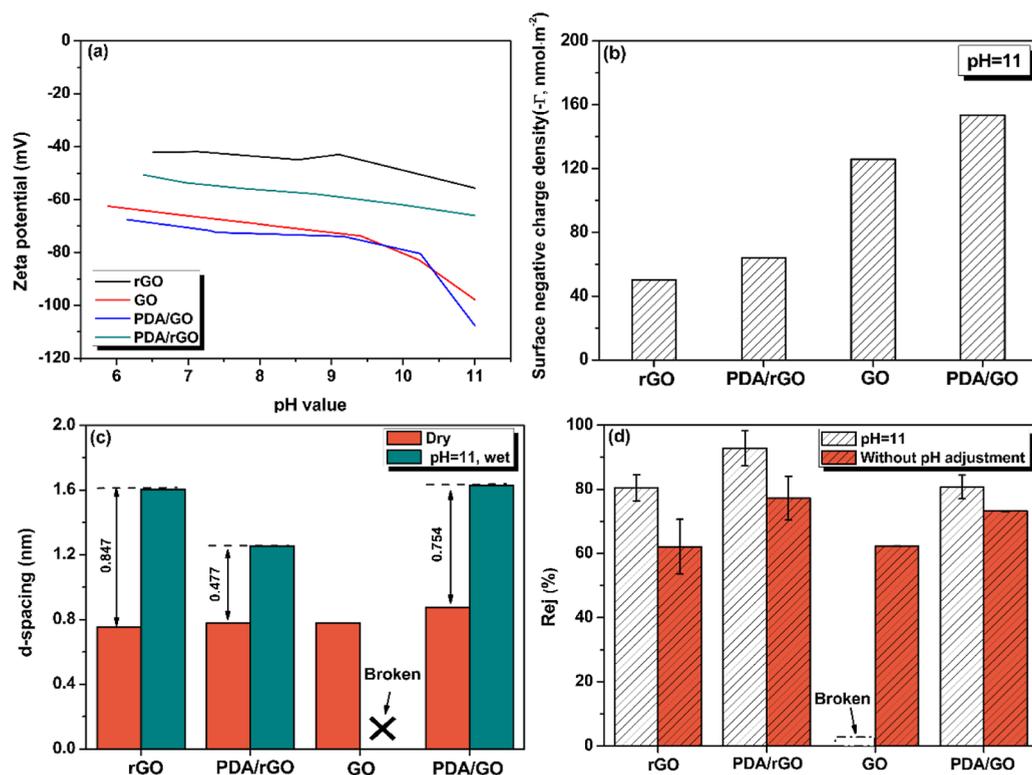
Figure 10. Zeta potential (a), calculated surface negative charge density (b), interlayer spacing (c), and Sr^{2+} rejection in pH 11 environment (d) of the GO, rGO, PDA/GO, and PDA/rGO membranes.

branes primarily arises from their intrinsic hydrophilicity, which is a result of the presence of oxygen-containing groups within their structure. To address this swelling concern when these membranes come into contact with aqueous solutions, a straightforward thermal reduction treatment is employed with the meticulous optimization of the treatment temperature.

Following the thermal reduction treatment, although the XRD diffraction peak of the membranes in the wet state still displayed a leftward shift compared to their dry state counterparts, the extent of this shift was notably mitigated (Figure S4). This observation signifies the effective mitigation of swelling. Specifically, the swelling of the membranes has decreased from 0.60 nm for the PDA/GO membrane without thermal reduction treatment (corresponding to the data point at 40 °C) to 0.33 and 0.29 nm for the PDA/rGO membranes treated at 80 and 120 °C (Figure 8a), respectively.

Furthermore, the successful mitigation of swelling is instrumental in enabling PDA/rGO membranes to effectively separate Sr^{2+}. Due to the effective mitigation of swelling achieved through thermal treatment, the interlayer spacing of PDA/rGO membranes remains below 1.16 nm even in the wet state. Consequently, the membrane subjected to thermal reduction treatment at 80 °C demonstrates improved Sr^{2+} rejection of 77.3% and is thus selected as the optimal condition for thermal reduction treatment.

3.3. Separation Mechanism of the PDA/rGO Membrane. As illustrated in Figure 8b, the PDA/rGO membranes subjected to thermal reduction treatment at 80 and 120 °C result in nearly identical interlayer spacing in their wet state. Nevertheless, there is a notable difference in Sr^{2+} rejection, with values of 77.3 for 80 °C and 64.7% for 120 °C. This discrepancy suggests that Sr^{2+} separation may not be solely dependent on size. Typically, membranes with a charged

surface, such as GO-based membranes, separate ions through a combination of size exclusion and charge repulsion effects.[39,40] Accordingly, the surface charge of these PDA/rGO membranes was characterized by zeta potential and analyzed by the calculation of surface charge density (Figure 9a and 9b).

It is evident that although the surfaces of all these membranes are negatively charged, the thermal reduction treatment at a higher temperature has resulted in a reduced surface charge density. In the context of cation Sr^{2+} separation (with nitrate as the anion), a more strongly negatively charged surface leads to a greater repulsion of NO_3^-. To maintain charge neutrality in the solution, Sr^{2+} ions are also rejected. Therefore, even though thermal reduction treatments at 80 and 120 °C have resulted in a similar interlayer spacing of the membrane, the higher charge density of the membrane treated at 80 °C favors greater Sr^{2+} rejection, whereas a more neutralized membrane surface after treatment at 120 °C leads to lower Sr^{2+} rejection.

The effect of surface charge during separation is further confirmed by evaluating Sr^{2+} rejection under various pH conditions using the PDA/rGO membrane subjected to 80 °C thermal treatment. As shown in Figure 9d, the negative charge density escalates with an increase in solution pH, intensifying the charge repulsion effect and consequently resulting in higher Sr^{2+} rejection.

The pH test was concluded at pH 11, driven by the analysis of the composition of Sr^{2+} aqueous solution. Beyond this point, Sr^{2+} undergoes partial precipitation, converting into $Sr(OH)^+$, thereby introducing inaccuracies in the calculation of the Sr^{2+} rejection (Figure 9c). Essentially, Sr^{2+} can indeed be removed from water by elevating the pH to exceptionally high levels; however, this method incurs a substantial consumption of chemicals and raises environmental concerns when the

resultant is a strongly alkaline solution. In contrast, membrane-based technology holds great promise for removing Sr^{2+} under more moderate conditions, a particularly relevant approach, given the inherently high pH levels sometimes found in real nuclear wastewater.

In short, the separation of Sr^{2+} by PDA/rGO membranes relies on the synergistic effect of size exclusion and charge repulsion. Membranes with an appropriate interlayer spacing and a high surface charge density are conducive to achieving exceptional Sr^{2+} rejection.

3.4. Advantages of the Combination of PDA Incorporation and Thermal Reduction Treatment.
A series of membranes were employed for comparative analysis, encompassing unmodified GO (GO), reduced GO without PDA incorporation (rGO), PDA-incorporated GO without thermal reduction treatment (PDA/GO), and membranes subjected to both PDA incorporation and thermal reduction treatment (PDA/rGO).

As elucidated earlier, Sr^{2+} separation is achieved through a synergistic effect combining size exclusion and charge repulsion. Consequently, the interlayer spacing and surface charge density of these membranes were measured and calculated.

The combination of PDA incorporation and thermal reduction treatment yields the smallest degree of swelling (Figures 10 and S5), even under pH 11 conditions, and features a relatively high surface charge density. The synergistic influence of these two critical factors culminates in the remarkable enhancement of Sr^{2+} separation performance compared to control samples subjected to different modification methods (Figure 10d).

An additional advantage stemming from the combination of PDA incorporation and thermal reduction treatment resides in the enhanced stability that it imparts upon the membrane, particularly when subjected to strongly alkaline environments. It is noteworthy that while GO-based membranes exhibit an impeccable layered structure, they tend to manifest swelling when exposed to highly alkaline solutions. This undesired expansion of interlayer spacing can be attributed to the augmented negative charge density within the system, engendering an increase in the repulsive forces between individual GO layers and thereby leading to the enlargement of interlayer spacing.

Our study has indicated that the swelling observed in the GO-based membranes can be effectively ameliorated through a judicious combination of PDA incorporation and thermal reduction treatment. Furthermore, the resultant modified membrane has demonstrated remarkable long-term stability when employed in Sr^{2+} ion separation under a highly alkaline environment characterized by a pH value of 11, as shown in Figure 11. While a limited number of studies have demonstrated the separation of larger dye molecules using GO-based membranes in challenging environments, it is pertinent to note that, to the best of our knowledge, there are no prior reports that have demonstrated the successful utilization of such membranes for separation of considerably smaller strontium ions under these stringent conditions.

4. CONCLUSIONS

In this study, an effective modification method for GO membranes has been developed to improve strontium (a major constituent in nuclear wastewater) separation performance and enhance the structural stability of the membrane in an alkaline
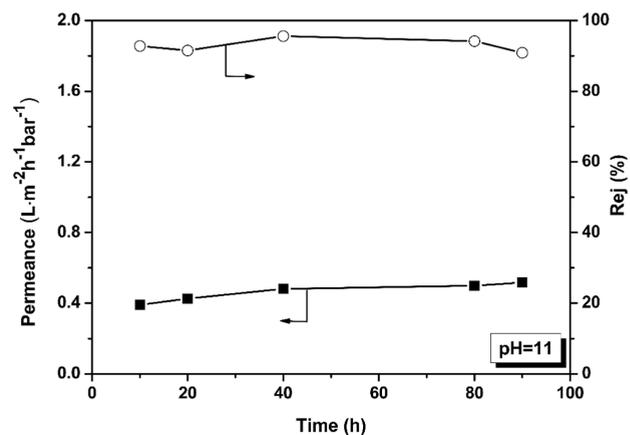

Figure 11. Long-term Sr^{2+} separation performance of PDA/rGO membranes at pH = 11 (the PDA/rGO membrane preparation conditions were: GO dosage = 0.042 mg·cm^{-2}, reaction time = 3 h, mass ratio of PDA/GO = 0.5:1 and thermal treatment temperature = 80 °C).

solution. The GO membrane was modified through the incorporation of PDA, followed by a subsequent thermal reduction treatment. By optimizing the modification procedure, the resultant membranes have successfully rejected the passage of strontium ions. The separation mechanism is investigated and determined to be a synergistic effect of size exclusion and charge repulsion; namely, an appropriate interlayer spacing and a high surface charge density favor better strontium separation. The modification method proposed in this study precisely regulated the interlayer spacing and enhanced the surface charge density of the GO membrane, resulting in an excellent strontium separation performance. In addition, the modified membranes have maintained steady strontium separation performance over an extended duration under a strongly alkaline environment with a pH of 11, indicating substantially enhanced structural stability by modification. These results highlighted the significant advantages offered by our modification strategy in enhancing the strontium separation performance of GO membranes.

■ ASSOCIATED CONTENT

⑤ Supporting Information

The Supporting Information is available free of charge at https://pubs.acs.org/doi/10.1021/acsomega.3c09712.

FTIR spectra of PDA/GO composite membranes with different reaction time; XRD patterns and the corresponding interlayer spacing of dry PDA/GO composite membranes with different reaction time; XRD patterns of PDA/GO composite membranes with different PDA/GO mass ratios in dry and wet states; XRD patterns of PDA/GO and PDA/rGO composite membrane in dry and wet states; XRD patterns of PDA/rGO, PDA/GO and rGO membrane in dry and wet states (pH = 11) (PDF)

■ AUTHOR INFORMATION

Corresponding Authors

Zhan Li − *Research Center for Membrane and Film Technology, Kobe University, Nada 657-8501 Kobe, Japan*; Email: lizhan@people.kobe-u.ac.jp

Hideto Matsuyama − *Research Center for Membrane and Film Technology, Kobe University, Nada 657-8501 Kobe, Japan; Department of Chemical Science and Engineering, Kobe University, Nada 657-8501 Kobe, Japan;* orcid.org/0000-0003-2468-4905; Email: matuyama@kobe-u.ac.jp

Authors

Chuang Li − *Research Center for Membrane and Film Technology, Kobe University, Nada 657-8501 Kobe, Japan; Department of Chemical Science and Engineering, Kobe University, Nada 657-8501 Kobe, Japan*

Zheng Wang − *Research Center for Membrane and Film Technology, Kobe University, Nada 657-8501 Kobe, Japan; Department of Chemical Science and Engineering, Kobe University, Nada 657-8501 Kobe, Japan*

Kecheng Guan − *Research Center for Membrane and Film Technology, Kobe University, Nada 657-8501 Kobe, Japan;* orcid.org/0000-0002-4924-7480

Yu-Hsuan Chiao − *Research Center for Membrane and Film Technology, Kobe University, Nada 657-8501 Kobe, Japan*

Pengfei Zhang − *Research Center for Membrane and Film Technology, Kobe University, Nada 657-8501 Kobe, Japan*

Ping Xu − *Research Center for Membrane and Film Technology, Kobe University, Nada 657-8501 Kobe, Japan*

Ralph Rolly Gonzales − *Research Center for Membrane and Film Technology, Kobe University, Nada 657-8501 Kobe, Japan;* orcid.org/0000-0002-2175-2944

Mengyang Hu − *Research Center for Membrane and Film Technology, Kobe University, Nada 657-8501 Kobe, Japan*

Zhaohuan Mai − *Research Center for Membrane and Film Technology, Kobe University, Nada 657-8501 Kobe, Japan*

Tomohisa Yoshioka − *Research Center for Membrane and Film Technology, Kobe University, Nada 657-8501 Kobe, Japan; Department of Chemical Science and Engineering, Kobe University, Nada 657-8501 Kobe, Japan;* orcid.org/0000-0002-7489-441X

Complete contact information is available at:
https://pubs.acs.org/10.1021/acsomega.3c09712

Notes

The authors declare no competing financial interest.

■ REFERENCES

(1) Komarneni, S.; Roy, R. Use of Gamma-Zirconium Phosphate for Cs Removal from Radioactive-Waste. *Nature* **1982**, *299* (5885), 707−708.

(2) Zhang, L.; Lu, Y.; Liu, Y. L.; Li, M.; Zhao, H. Y.; Hou, L. A. High flux MWCNTs-interlinked GO hybrid membranes survived in cross-flow filtration for the treatment of strontium-containing wastewater. *J. Hazard. Mater.* **2016**, *320*, 187−193.

(3) Xu, C.; Wang, J. C.; Chen, J. Solvent Extraction of Strontium and Cesium: A Review of Recent Progress. *Solvent Extr. Ion Exch.* **2012**, *30* (6), 623−650.

(4) Ding, S. Y.; Yang, Y.; Huang, H. O.; Liu, H. C.; Hou, L. A. Effects of feed solution chemistry on low pressure reverse osmosis filtration of cesium and strontium. *J. Hazard. Mater.* **2015**, *294*, 27−34.

(5) Sofronov, D.; Rucki, M.; Varchenko, V.; Bryleva, E.; Mateychenko, P.; Lebedynskiy, A. Removal of europium, cobalt and strontium from water solutions using MnO(OH)-modified diatomite. *J. Environ. Chem. Eng.* **2022**, *10* (1), 106944.

(6) Li, T. T.; He, F.; Dai, Y. D. Prussian blue analog caged in chitosan surface-decorated carbon nanotubes for removal cesium and strontium. *J. Radioanal. Nucl. Chem.* **2016**, *310* (3), 1139−1145.

(7) Shannon, M. A.; Bohn, P. W.; Elimelech, M.; Georgiadis, J. G.; Marinas, B. J.; Mayes, A. M. Science and technology for water purification in the coming decades. *Nature* **2008**, *452* (7185), 301−310.

(8) Huang, H. B.; Song, Z. G.; Wei, N.; Shi, L.; Mao, Y. Y.; Ying, Y. L.; Sun, L. W.; Xu, Z. P.; Peng, X. S. Ultrafast viscous water flow through nanostrand-channelled graphene oxide membranes. *Nat. Commun.* **2013**, *4*, 2979.

(9) Hu, M.; Zheng, S. X.; Mi, B. X. Organic Fouling of Graphene Oxide Membranes and Its Implications for Membrane Fouling Control in Engineered Osmosis. *Environ. Sci. Technol.* **2016**, *50* (2), 685−693.

(10) Xu, Z.; Sun, H. Y.; Zhao, X. L.; Gao, C. Ultrastrong Fibers Assembled from Giant Graphene Oxide Sheets. *Adv. Mater.* **2013**, *25* (2), 188−193.

(11) Dreyer, D. R.; Park, S.; Bielawski, C. W.; Ruoff, R. S. The chemistry of graphene oxide. *Chem. Soc. Rev.* **2010**, *39* (1), 228−240.

(12) Xia, S. J.; Ni, M.; Zhu, T. R.; Zhao, Y.; Li, N. N. Ultrathin graphene oxide nanosheet membranes with various d-spacing assembled using the pressure-assisted filtration method for removing natural organic matter. *Desalination* **2015**, *371*, 78−87.

(13) Han, Y.; Xu, Z.; Gao, C. Ultrathin Graphene Nanofiltration Membrane for Water Purification. *Adv. Funct. Mater.* **2013**, *23* (29), 3693−3700.

(14) Sun, P. Z.; Zhu, M.; Wang, K. L.; Zhong, M. L.; Wei, J. Q.; Wu, D. H.; Xu, Z. P.; Zhu, H. W. Selective Ion Penetration of Graphene Oxide Membranes. *ACS Nano* **2013**, *7* (1), 428−437.

(15) Sun, P. Z.; Zheng, F.; Zhu, M.; Song, Z. G.; Wang, K. L.; Zhong, M. L.; Wu, D. H.; Little, R. B.; Xu, Z. P.; Zhu, H. W. Selective Trans-Membrane Transport of Alkali and Alkaline Earth Cations through Graphene Oxide Membranes Based on Cation-pi Interactions. *ACS Nano* **2014**, *8* (1), 850−859.

(16) Joshi, R. K.; Carbone, P.; Wang, F. C.; Kravets, V. G.; Su, Y.; Grigorieva, I. V.; Wu, H. A.; Geim, A. K.; Nair, R. R. Precise and Ultrafast Molecular Sieving Through Graphene Oxide Membranes. *Science* **2014**, *343* (6172), 752−754.

(17) Wu, T.; Wang, Z.; Lu, Y.; Liu, S.; Li, H.; Ye, G.; Chen, J. Graphene Oxide Membranes for Tunable Ion Sieving in Acidic Radioactive Waste. *Adv. Sci.* **2021**, *8* (7), 2002717.

(18) Wang, S.; Liang, S. Acid response nanochannels of graphene oxide membranes for fast nuclide ions separation. *Sep. Purif. Technol.* **2024**, *328*, 125086.

(19) Ahn, E.; Gaiji, H.; Kim, T.; Abderrabba, M.; Lee, H. W.; Kim, B. S. Graphene oxide nanosheet as a two-dimensional polyelectrolyte: pH-responsive behavior of a multilayered nanomembrane. *J. Membr. Sci.* **2019**, *585*, 191−198.

(20) Lee, H.; Dellatore, S. M.; Miller, W. M.; Messersmith, P. B. Mussel-inspired surface chemistry for multifunctional coatings. *Science* **2007**, *318* (5849), 426−430.

(21) Lee, H.; Rho, J.; Messersmith, P. B. Facile Conjugation of Biomolecules onto Surfaces via Mussel Adhesive Protein Inspired Coatings. *Adv. Mater.* **2009**, *21* (4), 431−434.

(22) Hu, M.; Mi, B. X. Enabling Graphene Oxide Nanosheets as Water Separation Membranes. *Environ. Sci. Technol.* **2013**, *47* (8), 3715−3723.

(23) Xu, K.; Feng, B.; Zhou, C.; Huang, A. S. Synthesis of highly stable graphene oxide membranes on polydopamine functionalized supports for seawater desalination. *Chem. Eng. Sci.* **2016**, *146*, 159−165.

(24) Kong, F. X.; Liu, Q.; You, L.; Lu, P.; Liu, T.; Sun, G. D.; Wang, Y.; Chen, J. F. Facile preparation of dopamine mediated graphene oxide composite membranes with enhanced stability for nanofiltration: Structure, performance and stability. *Desalination* **2022**, *534*, 115778.

(25) Zhang, M. C.; Mao, Y. Y.; Liu, G. Z.; Liu, G. P.; Fan, Y. Q.; Jin, W. Q. Molecular Bridges Stabilize Graphene Oxide Membranes in Water. *Angew. Chem., Int. Ed.* **2020**, *59* (4), 1689−1695.

(26) Li, Y.; Zhao, W.; Weyland, M.; Yuan, S.; Xia, Y.; Liu, H. Y.; Jian, M. P.; Yang, J. D.; Easton, C. D.; Selomulya, C.; Zhang, X. W. Thermally Reduced Nanoporous Graphene Oxide Membrane for Desalination. *Environ. Sci. Technol.* **2019**, *53* (14), 8314−8323.

(27) Sun, P. Z.; Chen, Q.; Li, X. D.; Liu, H.; Wang, K. L.; Zhong, M. L.; Wei, J. Q.; Wu, D. H.; Ma, R. Z.; Sasaki, T.; Zhu, H. W. Highly efficient quasi-static water desalination using monolayer graphene oxide/titania hybrid laminates. *NPG Asia Mater.* **2015**, *7*, No. e162.

(28) Li, Y.; Yuan, S.; Xia, Y.; Zhao, W.; Easton, C. D.; Selomulya, C.; Zhang, X. W. Mild annealing reduced graphene oxide membrane for nanofiltration. *J. Membr. Sci.* **2020**, *601*, 117900.

(29) Jang, J. H.; Woo, J. Y.; Lee, J.; Han, C. S. Ambivalent Effect of Thermal Reduction in Mass Rejection through Graphene Oxide Membrane. *Environ. Sci. Technol.* **2016**, *50* (18), 10024−10030.

(30) Wei, Y.; Cao, L.; Zhu, J.; Wang, L.; Yao, H.; Sun, H.; Xia, X.; Zhao, H.; Ji, T.; Ni, S.; Zheng, J.; Yang, Y.; Zhou, F.; Chen, L. Radioactive strontium ions sieving through reduced graphene oxide membrane. *J. Membr. Sci.* **2024**, *689*, 122181.

(31) Liu, L. F.; Zhou, Y. S.; Xue, J.; Wang, H. H. Enhanced antipressure ability through graphene oxide membrane by intercalating g-C3N4 nanosheets for water purification. *AIChE J.* **2019**, *65* (10), No. e16699.

(32) Takagi, R.; Hori, M.; Gotoh, K.; Tagawa, M.; Nakagaki, M. Donnan potential and zeta-potential of cellulose acetate membrane in aqueous sodium chloride solutions. *J. Membr. Sci.* **2000**, *170* (1), 19−25.

(33) Stankovich, S.; Dikin, D. A.; Piner, R. D.; Kohlhaas, K. A.; Kleinhammes, A.; Jia, Y.; Wu, Y.; Nguyen, S. T.; Ruoff, R. S. Synthesis of graphene-based nanosheets via chemical reduction of exfoliated graphite oxide. *Carbon* **2007**, *45* (7), 1558−1565.

(34) Zhao, Z. W.; Li, J. X.; Wen, T.; Shen, C. C.; Wang, X. K.; Xu, A. W. Surface functionalization graphene oxide by polydopamine for high affinity of radionuclides. *Colloids Surf., A* **2015**, *482*, 258−266.

(35) Huang, H. H.; Joshi, R. K.; De Silva, K. K. H.; Badam, R.; Yoshimura, M. Fabrication of reduced graphene oxide membranes for water desalination. *J. Membr. Sci.* **2019**, *572*, 12−19.

(36) Zhang, M.; Mao, Y.; Liu, G.; Liu, G.; Fan, Y.; Jin, W. Molecular Bridges Stabilize Graphene Oxide Membranes in Water. *Angew. Chem., Int. Ed.* **2020**, *59* (4), 1689−1695.

(37) Guan, K. C.; Guo, Y. A.; Li, Z.; Jia, Y. D.; Shen, Q.; Nakagawa, K.; Yoshioka, T.; Liu, G. P.; Jin, W. Q.; Matsuyama, H. Deformation constraints of graphene oxide nanochannels under reverse osmosis. *Nat. Commun.* **2023**, *14* (1), 1016.

(38) Hu, M.; Mi, B. X. Layer-by-layer assembly of graphene oxide membranes via electrostatic interaction. *J. Membr. Sci.* **2014**, *469*, 80−87.

(39) Huang, Q. B.; Liu, S.; Guo, Y. A.; Liu, G. P.; Jin, W. Q. Separation of mono-/di-valent ions via charged interlayer channels of graphene oxide membranes. *J. Membr. Sci.* **2022**, *645*, 120212.

(40) He, L.; Dumée, L. F.; Feng, C. F.; Velleman, L.; Reis, R.; She, F. H.; Gao, W. M.; Kong, L. X. Promoted water transport across graphene oxide-poly(amide) thin film composite membranes and their antibacterial activity. *Desalination* **2015**, *365*, 126−135.